Control of acousto-optic mode locker by means of electronic matching circuit

Grigorii D. Slinkov, Sergey N. Mantsevich, Vladimir I. Balakshy, Leonid. N. Magdich, Alexander S. Machikhin

***Abstract*—An acousto-optic (AO) mode locker (AOML) operating in a standing wave mode has a fixed working frequency, defined by the length of the crystal, which makes it prone to temperature variations. In this study we examine the effect of the electrical matching circuit parameters on the acoustic resonances and AO diffraction in the AOML both theoretically and experimentally. Acoustical and electrical models of the AOML are introduced. We outline the ways of utilizing this effect for compensation of that ill thermal influence. Our analysis allows to broaden the temperature and driving power domains of an AO mode locker's reliable operation without a bulky heat sink or other complicated temperature stabilization systems.**

***Index Terms*—acousto-optics, mode locking, electrical matching circuit, standing wave, acousto-optical mode locker**

I. INTRODUCTION

Acousto-optical methods of optical radiation control are widely applied in various branches of modern optoelectronics [1, 2, 3, 4]. Among the variety of AO devices there are acousto-optical modulators (AOMs) [3], one of their peculiar applications being active locking of longitudinal laser modes. This technique allows to acquire an evenly spaced train of short and powerful pulses from a conventional CW laser [5, 6, 7, 8, 9]. Mode locking can be implemented through amplitude modulation of optical radiation inside the laser's optical cavity with a frequency f equal to the inter-modal distance of that cavity $c/2L_l$, where c is the speed of light and L_l is cavity length. Most of the AOMs utilized for mode locking operate in a standing wave mode, since it is a simpler and much more power-effective way, as compared to driving the AOM with a modulated RF signal. Thus, ultrasound frequency f must also meet standing wave condition, determined by the AOM's crystal length L_s:

$$f = f_a = (V_s n)/(2L_s), n \in \mathbb{Z}, \tag{1}$$

where V_s is acoustic wave velocity. Therefore, the heating of the crystal caused by absorption of acoustic energy hinders the AO mode locker operation. Interestingly, the way the heating of the crystal affects operation of an AOML differs completely from what is observed for AO tunable filters and deflectors [10, 11, 12, 13, 14]. Thermal expansion of the crystal breaks the standing wave condition (1) by increasing L_s, which, in turn, leads to modulation effectiveness drop. This problem we address in terms of temperature variation causing acoustic resonance frequency f_a shift. Sophisticated AO cell temperature stabilization systems, as well as plain water cooling may be applied to reduce this effect [15].

We provide Fig. 1 in order to illustrate the described thermal frequency shift. Here, the electrical power absorption coefficient A_P of an AOML is plotted against driving signal frequency,

$$A_P = 1 - R_P = 1 - \frac{P_{refl}}{P_{in}}, \tag{2}$$

where R_P is the power reflection coefficient, P_{in} is incident power, P_{refl} is reflected power.

Two curves are presented in the figure. The one signed as "cold" was obtained at a relatively low driving signal power (0.5 W). Then the power was raised up to 3 W, and after a homogeneous temperature distribution has been reached, "hot" measurements were performed. Absorption of acoustic energy in crystal resulted in heating of its body from 20^oC to 28^oC. This caused a frequency shift of about 14 kHz, which, in its turn, decreased the electrical power absorption coefficient (electrical matching effectiveness) by 20%.

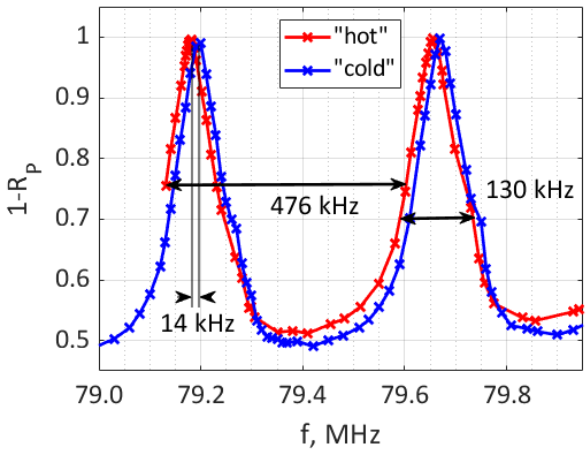

Fig. 1: Electrical power absorption coefficient of an AOML at different temperatures ($\Delta T = 8^o$ C). Resulting resonance frequency shift is 14 kHz

However, a specific method for compensating this thermal shift exists. It is based on the dependence of acoustic resonance frequency f_a on the parameters of an electrical matching circuit (EMC) of an AOML, first reported in [16]. It has been shown [17, 18] that it is possible to adjust the acoustic

G. D. Slinkov, S. N. Mantsevich and V. I. Balakshy are with Physics Department, M.V. Lomonosov Moscow State University, 1 Leninskie Gory, Moscow, Russia, 119991.

L. N. Magdich is with Stel'makh Research and Development Institute "Polyus", 3 Vvedenskogo, Moscow, Russia, 117342

A. S. Machikhin is with Russian Academy of Sciences Scientific and Technological Center of Unique Instrumentation, 15 Butlerova, Moscow, Russia, 117342

Corresponding author: G. D. Slinkov, kanttheisland@gmail.com

resonance frequency within certain limits through variation of the EMC parameters (e.g. by replacing a capacitor).

An electrical matching circuit is an integral component of any acousto-optic device. Its purpose is to facilitate the piezoelectric transducer in transforming the electrical power received from the driver into acoustic power in a desired frequency domain [19, 20]. For example, appropriate matching circuit could widen the frequency band of an AOTF or enhance the modulation depth of an AOM. In this study we examine the effects of the EMC's electrical parameters on the characteristics of acoustic resonances and AO diffraction of the AOML and outline the ways of applying it for compensation of that thermal frequency shift both theoretically and experimentally. Our analysis paves the way for broadening the temperature and power domains of acousto-optic mode locker reliable operation, which does not require an introduction of a heat sink.

II. Modelling

An acousto-optical device ultimately incorporates two parts - the electrical part (the matching circuit) and the acoustical one (the AO cell). The acoustical part also consists of a crystal and a piezo-transducer. Under the current section we will consider these parts separately.

A. AO cell acoustic model

To begin with, let us introduce an acoustical model of an AO cell (Fig. 2). We assume that the cell consists of two infinite material layers, one being lithium niobate, the piezo-transducer, confined between planes $z = -h$ and $z = 0$, and the other one being crystalline quartz, the medium for acousto-optic interaction, confined between $z = 0$ and $z = l$. We examine a pair of plane acoustic waves, the incident u_1 and the reflected one u_2:

$$u_1(z,\Omega) = A_1^+ e^{i(\Omega t - k_1 z)} + A_1^- e^{i(\Omega t + k_1 z)} \quad (3)$$

$$u_2(z,\Omega) = A_2^+ e^{-\alpha z} e^{i(\Omega t - k_2 z)} + A_2^- e^{\alpha z} e^{i(\Omega t + k_2 z)}, \quad (4)$$

where Ω - frequency, α - absorption coefficient, $k_{1,2}$ - wave vectors, A_1^+ A_1^- - amplitudes of acoustic waves in piezo-transducer medium, A_2^+ A_2^- - amplitudes of acoustic waves in crystal[1].

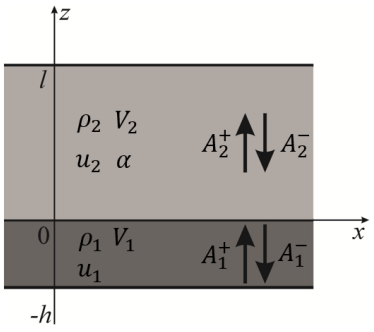

Fig. 2: Acoustical model of the AO cell

[1]Here and below all x_1 indices correspond to acoustic waves in piezo-transducer, and all x_2 indices correspond to acoustic waves in the crystal

Propagation of these plane waves is governed by the following equations, which take piezo-effect into account:

$$\rho_2 \frac{d^2 u_2}{dt^2} = \frac{dT_2}{dz} \qquad T_2 = c_2 \frac{du_2}{dz} \quad (5)$$

$$\rho_1 \frac{d^2 u_1}{dt^2} = \frac{dT_1}{dz} \qquad T_1 = c_1 \frac{du_1}{dz} - eE \quad (6)$$

$$E = -\frac{d\phi}{dz} \qquad \frac{dD}{dz} = 0 \qquad D = \varepsilon E + e\frac{du_1}{dz}, \quad (7)$$

where $u_{1,2}$ is displacement, $T_{1,2}$ - stress, $\rho_{1,2}$ - mechanical density, $c_{1,2}$ - elastic module, ϕ - scalar electric potential, ε - static electric permeability, e - electron charge.

The boundary conditions for solving presented equations (5-7) are the following:

$$\phi(0) = 0 \qquad \phi(-h) = U_e e^{i\Omega t} \quad (8)$$

for the voltage on the electrodes of the piezo-transducer,

$$T_1(-h) = 0 \qquad T_2(l) = 0 \quad (9)$$

for "free" boundaries of the crystal and the piezo-transducer, and

$$u_1(0) = u_2(0) \qquad T_1(0) = T_2(0). \quad (10)$$

for the boundary between the crystal and the transducer.

By solving equations (5-7) with boundary conditions (8-10), one can obtain following expressions:

$$A_2^+(U_e, F) = U_e \cdot (1 - cosF)Q/G \quad (11)$$

for the amplitude of the acoustic wave at the end face of the crystal, where U_e - voltage on the electrodes of the piezo-transducer. And

$$Z_e^{-1}(F) = \frac{i\Omega C_0 F cosF}{K}\Big(1 - k^2(1 - cosF)^2(E+1)/G\Big) \quad (12)$$

for electric impedance of the AO cell, where C_0 is static capacity of the piezo-transducer. Following substitutions utilized:

$$G = \frac{Z_a}{F}\Big((\beta + jF)(E-1)K + \\ + (E+1)(FsinF - 2k^2(1 - cosF))\Big) \quad (13)$$

$$K = FcosF - k^2 sinF \quad (14)$$

$$E = exp\left[-2\gamma(\beta + iF)\right] \quad (15)$$

$$F = \frac{\Omega \cdot h}{V_1} \qquad \beta = \frac{\alpha V_2 h}{V_1} \qquad \gamma = \frac{V_1 l}{V_2 h} \quad (16)$$

$$Z_a = \frac{\rho_2 V_2}{\rho_1 V_1} \qquad Q = \frac{k}{V_1}\sqrt{\frac{\varepsilon}{\rho_1}} \qquad k = \frac{e^2}{\varepsilon V_1}, \quad (17)$$

where Ω is driving signal frequency, $V_{1,2}$ - ultrasound velocity, $\rho_{1,2}$ - mechanical density in respective media, ε - static electric permeability, e - electron charge.

The key characteristics of the AOML that can be calculated with presented theory are the acoustic wave amplitude A_2^+ (11), since resulting diffraction efficiency, which determines

modulation depth, is proportional to the power of the acoustic signal within the crystal:

$$P_A \sim (A_2^+)^2, \tag{18}$$

and the electrical impedance of the AO cell (12), since it is essential for deriving the voltage on the electrodes of the piezo-transducer U_e, which comprises the acoustic wave amplitude expression (11).

B. Electrical matching circuit

A conventional way to analyse an electrical matching circuit of an AO device is to simply lay out equations for voltages and currents in the circuit [19, 21]. However, a more general approach exists [22, 23]. The electrical matching circuit of an acousto-optic device is usually a simple two-port network (quadripole). This allows us to apply the A-matrix (or, in some sources, ABCD-matrix) formalization to describe its properties. This method was first applied to analyse the operation of an AO tunable filter in [23] and was a success at predicting the difference between operational bandwidths of an individual matching circuit and an AO filter as whole. Within described formalization, input and output voltages and currents (Fig. 3, blue color) of a quadripole are related by a transmission matrix:

$$\begin{pmatrix} U_1 \\ I_1 \end{pmatrix} = \begin{pmatrix} A & B \\ C & D \end{pmatrix} \begin{pmatrix} U_2 \\ -I_2 \end{pmatrix} \tag{19}$$

The voltaic transmission characteristic of a quadripole in this formalization is given by equation:

$$H = \frac{U_e}{U_0} = \left[A + \frac{B}{Z_e} + Cr_i + \frac{Dr_i}{Z_e} \right]^{-1}, \tag{20}$$

where U_0 is driver output voltage, r_i is driver output impedance, Z_e is the electrical impedance of the AO cell, given by eq. (12), U_e is the voltage on the electrodes of the AO cell (Fig. 3).

This H-characteristic (20), unfortunately, does not account for the fact that the load strongly affects output voltage of the driver: it is only guaranteed to provide required voltage when the load impedance equals the output impedance of the driver (50 Ω). This proved to be important for AO tunable filters [20], and is truly critical for such a multi-resonant load as an AOML. However, the quadripole formalization provides a so-called "effective transmission characteristic" which surpasses this limitation:

$$H_{eff} = 2\frac{U_e}{U_0}\sqrt{\frac{r_i}{Z_e}} \tag{21}$$

This characteristic is introduced through normalization of the conventional characteristic H by the maximum voltage that the driver could deliver to a perfectly matched load (see App. A for detail). We should note that it is proportional to a square root of the power delivered to the load:

$$P_e = \frac{U_e^2}{Z_e}$$

In accordance with presented theory, dependence of the acoustic wave amplitude on the parameters of the electrical matching circuit is provided by the U_e factor in Eq. (11), which represents voltage on the electrodes of the piezo-transducer, which, in turn, is governed by the electrical properties of the AOML - impedance of the AO cell (12), topology and parameters of the electrical matching circuit presented in Fig. 3. Considering driver output voltage constant, we can substitute H_{eff} (21) into Eq. (11) at the place of U_e, which will give us the resulting acoustic wave amplitude. This way, since the EMC affects not only amplitude but also the phase of a transmitted signal, it is clear that the acoustical resonances of the AO cell indeed can be affected by the parameters of the electrical matching circuit.

C. AO cell under study

In order to have means of comparing theoretically calculated characteristics with those measured experimentally, we introduce the following parameters of an actual AOML which underwent the successive experiments. The topology of a matching circuit is presented in Fig. 3, initial (factory-chosen) parameters were $C_m = 120$ pF and $L_m = 50.8$ nH. Piezo-transducer is lithium niobate under $Y+36^o$ cut, exciting longitudinal wave with ultrasound velocity $V_1 = 7.34 \cdot 10^5$ cm/s, two plates of $4.5 \times 20 \times 0.45$ mm, connected parallel, resulting static capacity $C_0 = 330$ pF. AO crystal is $45 \times 8 \times 6$ mm block of crystalline quartz, acoustic wave velosity $V_2 = 5.75 \cdot 10^5$ cm/s. Since our crystal effectively constitutes an acoustic Fabri-Perrot resonator, we were able to clarify its length $l = 6.04$ mm by measuring the free spectral range (FSR$= c/2L$) of such resonator (e.g. Fig. 1). We were also forced to modify the absorption coefficient α to achieve coincidence between the calculated acoustic resonance width and the experimentally measured one.

D. Simulation results

With the provided data it is possible to simulate the propagation of an acoustic wave in crystal, and calculate its amplitude at various frequencies. We summarize the results of the simulation by plotting the position - frequency - (Fig. 4a) and the height - acoustic wave power - (Fig. 4b) of a single resonant peak, obtained for different values of C_m and L_m.

Both plots reveal non-monotonic dependencies on the parameters of the EMC. For the sake of thermal frequency shift compensation, one can use these plots to choose an area where high acoustic power coincides with strong frequency gradient. It is also worth noting that the high power area is limited, which reveals the initial necessity of electrical matching.

III. Diffraction efficiency measurements

In order to test results presented in sec. II-D, diffraction efficiency measurements were performed. Experimental setup scheme is presented in Fig. 5: laser (1) beam is directed with a mirror (2) at the AOML (3), mounted on a rotation stage (4). All measurements were performed in the zeroth order of diffraction, higher order beams (+1 and -1, since a standing wave excites both) were absorbed by the aperture (5). A polarizer (6) is applied to decrease intensity of the beam

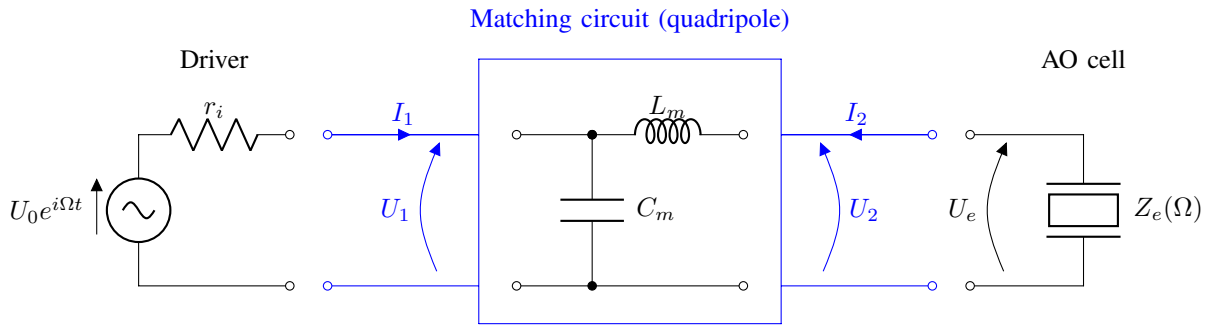

Fig. 3: Equivalent electrical scheme of an acousto-optic mode locker connected to a RF driver with output impedance r_i. The electrical impedance of the AO cell Z_e is given by eq. (12)

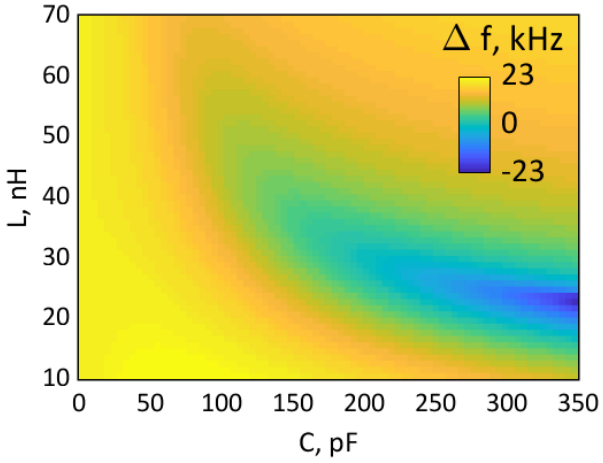

(a)

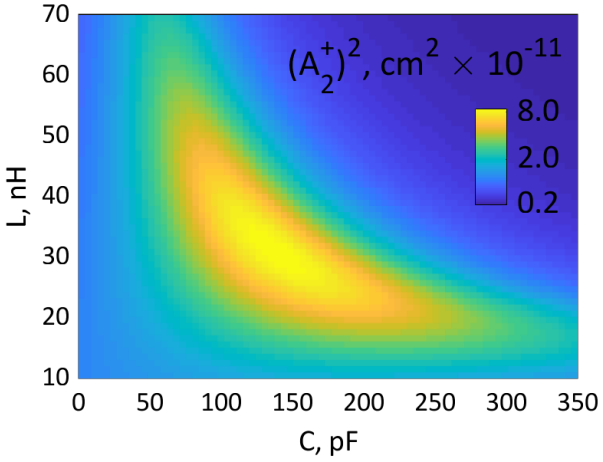

(b)

Fig. 4: Simulated resonant frequency shift (a), $\Delta f = f - f_0$, $f_0 = 80.29$ MHz; (b) - simulated acoustic wave amplitude square at resonant frequency, $P_A \sim (A_2^+)^2$

to avoid oversaturation of a photo detector (8). The beam is focused on the photo detector by a lens (7). RF generator operating in a frequency sweep mode allowed us to observe diffraction efficiency peaks with the oscilloscope.

Obtained results are presented in Fig. 6. Comparing them with theoretical ones requires taking a cross-sections of the surfaces in Fig. 4a and 4b by a $L_m = const$ plane. As we can see, the magnitude of the frequency shift surpasses 20 kHz as C_m is varied from 50 to 140 pF. This is sufficient for overcoming the thermal shift (Fig. 1) which has been established to have magnitude of about 14 kHz. The peak value of the diffraction efficiency also changes, thus our technique may be inapplicable in cases where high modulation depth is required. Nevertheless, it does not drop lower than 35%, which is quite enough for the purpose of mode locking.

We should point out that direct comparison between theoretical and experimental data is hardly possible. Firstly, our model is capable of reproducing the distance between resonant peaks, but not their actual positions. Secondly, electric circuits operating at high frequencies tend to suffer from parasitic effects: any wire, however slight its curvature, will have its own inductivity and capacity, which will both contribute into the resulting impedance. This effect is problematic to account for apart from knowing that the resulting capacity/inductivity of any element will be higher than those of an isolated element at low frequencies.

IV. Electrical power reflection coefficient measurements

One may propose a simpler way for measuring resonant characteristics of an AOML. Due to the direct piezo-effect (as opposed to inverse piezo-effect which is utilized to excite acoustic waves in AO devices), acoustic wave reflection at the end face of the crystal results in a reflected electric signal. This peculiarity is also revealed in the resonant nature of the electric impedance of the AO cell (12). Therefore, it must be possible to derive the desired frequency shift by measuring electrical response of the AOML. It is intuitively clear that the lower values of the power reflection coefficient R_P should correspond to higher acoustical power circulating within the crystal, since bulk losses at relatively low acoustic power levels are linear. In other words, one should be able to measure the acoustic resonance frequency shift by following the position of

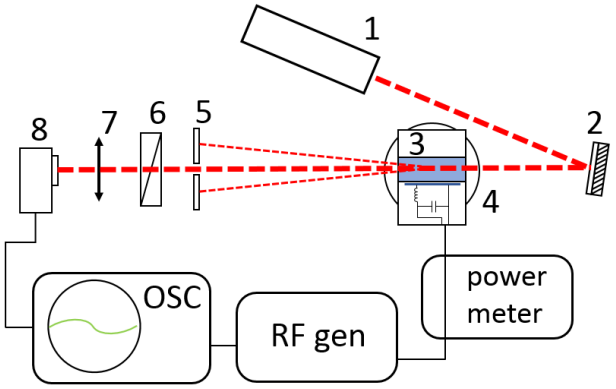

Fig. 5: Experimental setup scheme: 1 - laser, 2 - mirror, 3 - AOML, 4 - turning stage, 5 - aperture, 6 - polarizer, 7 - lens, 8 - photo detector

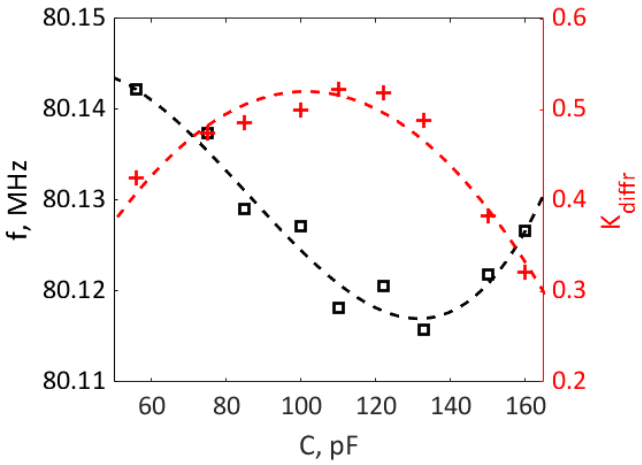

Fig. 6: Experimentally measured position and height of the diffraction efficiency peak at various matching circuit capacities; $L = 39$ nH

a single downwards pointing peak while changing the EMC parameters. Described approach lies within the conventional paradigm for AO devices characteristics evaluation (bandwidth, power transformation effectiveness etc.), which relies on standing wave ratio (SWR) measurements[2].

In order to test this hypothesis, electrical reflection coefficient R_P (s_{11} element of the scattering matrix) of the AOML was measured by means of a vector network analyzer (VNA), which is basically a phase-sensitive electric spectrum analyzer with an in-built generator. The result is presented in Fig. 7. Resonant peak (if a curve showing such a flat top could be called "peak") shows a really specific behaviour. Firstly, full span of the frequency shift approaches the FSR of the acoustic resonator (crystal): 476 kHz. Secondly, values of C_m, corresponding to higher resonant frequency gradient (faster

[2]Standing wave ratio measurements are equivalent to power reflection coefficient (R_P) measurements in our case, since there is a simple relation between them, which preserves the positions of the peaks: $SWR = \frac{1+\sqrt{R_P}}{1-\sqrt{R_P}}$

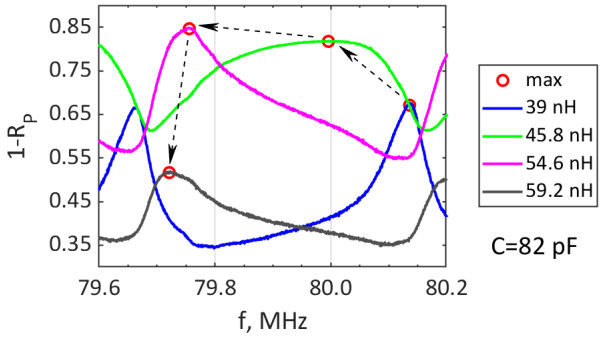

Fig. 7: Experimentally measured electric power absorption coefficient, plotted against frequency at different L_m values. The red dots identify the position of the "peak".

shift with change of L_m) also bear larger peak height (greater power absorption), and lower Q-factor (higher peak width).

This result shows that acoustical (Fig. 6) and electrical (Fig. 7) resonant characteristics are not as correlated as we supposed. Namely, electric signal resonances may not at all coincide with acoustic ones. From this we conclude that measuring only the electrical characteristics is not an adequate way for addressing the problem of electrical matching of a standing wave mode acousto-optic modulator. The discovered mismatch turns out to be in accordance with incompatibilities of AO tunable filters bandwidth measurements, recently reported in [23, 24]. Its shown there that standing wave ratio measurements inevitably result in higher bandwidth values than direct diffraction efficiency measurements.

V. Discussion and Conclusions

In this study we have shown, both theoretically and experimentally, that resonant characteristics of an AOML depend strongly on the parameters of its electronic matching circuit. Furthermore, we have shown that the effect of acoustical resonance frequency EMC-tuning is sufficient for the purpose of thermal frequency shift compensation. Good qualitative correspondence between experimental and theoretical frequency and diffraction efficiency dependencies is achieved. Utilization of the effective transmission characteristic (21), which proved to be crucial for this correspondence, is not, in fact, a novelty. It actually accounts for the fact that it is not the maximum voltage that is required to achieve maximum acoustical wave amplitude, as (11) infers, but rather the maximum electrical power.

We also consider one of our main results being the fact that electrical resonances of an AOML may not coincide with acoustic ones, as comparison between characteristics obtained via electronic measurements and optical ones had shown. Combining this observation with what is established for AO tunable filters [23, 24] and also keeping in mind that optical radiation control is the actual purpose of an acousto-optical device, we conclude that optical measurements, and not electrical ones, are the only correct approach for measuring the characteristics of an AO device. For example, in case of an

AOML, neglecting this principle may lead to a conclusion that electrical matching could shift acoustic resonance frequency within a full FSR (Fig. 7), which is not the case, as optical measurements have shown (Fig. 6). Moreover, existence of EMC configurations under which high electrical power absorption coincides with low acoustical signal power strongly indicates that there are some unaccounted losses in our AO device model, their source is located between the crystal and the driver, into which category fall the electrical matching circuit and the piezo-transducer.

ACKNOWLEDGEMENTS

This paper was supported by Russian Science Foundation (RSF) grant 19-19-00606

APPENDIX A
EFFECTIVE TRANSMISSION CHARACTERISTIC OF A QUADRIPOLE

Following [25] we will introduce the notion of an effective transmission characteristic of a quadripole as follows:

1) Maximum power delivered to a passive load on direct connection to the driver is
$$max[P_e] = \frac{U_0^2}{4r_i}$$
2) Maximum power in the load can not be higher than
$$P_e \leq \frac{max[U_e]^2}{Z_e}$$
3) From equality of presented values we determine magnitude of a normalization voltage on the load
$$max[U_e] = \frac{1}{2}U_0\sqrt{\frac{r}{Z_e}}$$
4) Then the effective transmission characteristic will be:
$$H_o = \frac{U_e}{max[U_e]} = 2\frac{U_e}{U_0}\sqrt{\frac{r_i}{Z_e}}$$

Considering Eq.(20), we can conclude that

$$H_o = H \cdot 2\sqrt{\frac{r_i}{Z_e}}$$

REFERENCES

[1] L. N. Magdich, V. Y. Molchanov, Acoustooptic devices and their applications, CRC Press, 1989.

[2] A. Yariv, P. Yeh, Optical waves in crystals, volume 5, Wiley, New York, 1984.

[3] V. I. Balakshy, V. N. Parygin, L. E. Chirkov, Physical principles of acousto-optics, Radio i Svyaz, Moscow, 1985.

[4] N. Berg, J. Pellegrino, Acousto-Optic Signal Processing, Marcel Dekker, New York, 1995.

[5] J. Herrmann, B. Wilhelmi, Laser fur ultrakurze Lichtimpulse: Grundlagen und Anwendungen, Physik-Verlag, Berlin, 1984.

[6] D. Kuizenga, A. Siegman, FM and AM mode locking of the homogeneous laser-part i: Theory, IEEE Journal of Quantum Electronics 6(11) (1970) 694–708.

[7] S. Basu, R. Byer, Continuous-wave mode-locked nd: glass laser pumped by a laser diode, Optics letters 13(6) (1988) 458–460.

[8] L. E. Hargrove, L. F. Richard, M. A. Pollack, Locking of hene laser modes induced by synchronous intracavity modulation, Applied Physics Letters 5(1) (1964) 4–5.

[9] A. E. Siegman, D. D. Kuizenga, Active mode-coupling phenomena in pulsed and continuous lasers, Opto-electronics 5 (1974) 43–66.

[10] V. I. Balakshy, V. B. Voloshinov, V. A. Karasev, V. Y. Molchanov, V. Semenkov, Compensation of thermal effects in acousto-optic deflector, Proc. SPIE 2713 (1996) 164–171.

[11] S. N. Mantsevich, T. V. Yukhnevich, V. B. Voloshinov, Examination of the temperature influence on the acousto-optic filters performance, Optics and Spectroscopy 122 (2017) 675–681.

[12] S. N. Mantsevich, O. I. Korablev, Y. I. Kalinnikov, A. Y. Ivanov, A. V. Kiselev, Wideaperture TeO2 AOTF at low temperatures: operation and survival, Ultrasonics 59 (2015) 50–58.

[13] S. N. Mantsevich, O. I. Korablev, Y. I. Kalinnikov, A. Y. Ivanov, A. V. Kiselev, Examination of temperature influence on wide-angle paratellurite crystal acousto-optic filters operation, Acta Physica Polonica A 127 (2015) 43–45.

[14] E. Dekemper, J. Vanhamel, B. Van Opstal, D. Fussen, V. B. Voloshinov, Influence of driving power on the performance of UV KDP-based acousto-optical tunable filters, Journal of Optics 17 (2015) 075404.

[15] E. Kruger, T. Kersebom, Resonance-tracking servo for an acousto-optic modulator, Review of scientific instruments 65.8 (1994) 2482–2488.

[16] L. N. Magdich, V. I. Balakshy, S. N. Mantsevich, Electronic tuning of acoustic resonances in acousto-optic mode lockers, Applied acoustics 112 (2016) 217–220.

[17] L. N. Magdich, V. I. Balakshy, S. N. Mantsevich, Electronic frequency tuning of the acousto-optic mode-locking device of a laser, Acoustical Physics 63 (2017) 645–651.

[18] V. I. Balakshy, L. N. Magdich, S. N. Mantsevich, Electrical control of the frequencies of a FabriPerrot acoustic resonator, Bulletin of the Russian Academy of Sciences: Physics 82 (2018) 459–465.

[19] I. B. Belikov, V. B. Voloshinov, A. B. Kasyanov, V. N. Parygin, Acoustooptic cell transducer broad-band matching, Izvestiya Vysshikh Uchebnykh Zavedenii Radioelektronika 31 (1988) 30–35.

[20] V. I. Balakshy, B. B. J. Linde, A. N. Vostrikova, Acousto-optic interaction in a non-homogeneous acoustic field excited by a wedge-shaped transducer, Ultrasonics 48 (2008) 351–356.

[21] Y. Chen, Acoustical transmission line model for ultrasonic transducers for wide-bandwidth application, Acta Mechanica Solida Sinica 23 (2010) 124134.

[22] E. K. Sitting, Effects of bonding and electrode layers on the transmission parameters of piezoelectric transducers used in ultrasonic digital delay lines, IEEE Trans. Son.

Ultrason. 16 (1969) 2–10.
[23] P. Maák, T. Takács, A. Barőcsi, E. Kollár, P. Richter, Thermal behavior of acousto-optic devices: Effects of ultrasound absorption and transducer losses, Ultrasonics 51(4) (2011) 441–451.
[24] J. Vanhamel, E. Dekemper, V. B. Voloshinov, J. Neefs, D. Fussen, Electrical bandwidth of an AOTF transducer as a function of the optical diffraction efficiency, JOSAA 36 (2019) 1361–1366.
[25] V. Fusco, Microwave circuits: analysis and computer-aided design, Prentice-Hall, 1987.